PERGAMON

International Journal of Heat and Mass Transfer 45 (2002) 1915–1931

International Journal of HEAT and MASS TRANSFER

www.elsevier.com/locate/ijhmt

Measurement and numerical analysis of freezing in solutions enclosed in a small container

Ramachandra V. Devireddy [a,d,1], Perry H. Leo [b], John S. Lowengrub [c], John C. Bischof [d,*]

[a] *Department of Chemical Engineering, Materials Research Science and Engineering Center, University of Minnesota, Minneapolis, MN 55455, USA*

[b] *Aerospace Engineering and Mechanics, Minneapolis, MN 55455, USA*

[c] *School of Mathematics, University of Minnesota, Minneapolis, MN 55455, USA*

[d] *Bioheat and Mass Transfer Laboratory, Department of Mechanical Engineering, University of Minnesota, 111 Church Street SE, Minneapolis, MN 55455, USA*

Received 9 March 2001; received in revised form 19 June 2001

Abstract

The latent heat of fusion, L of the cryobiological media (a solute laden aqueous solution) is a crucial parameter in the cryopreservation process and has often been approximated to that of pure water (~335 mJ/mg). This study experimentally determines the magnitude and dynamics of latent heat during freezing of 14 different pre-nucleated solute laden aqueous systems using a differential scanning calorimeter (DSC-Pyris 1). The latent heat of the solutions studied is found to be significantly less than that of pure water and is dependent on both the 'amount' and 'type' of solutes (or solids) in solution. DSC experiments are also performed at 1, 5 and 20 °C/min in five representative cryobiological media to determine the kinetics of ice crystallization. The total magnitude of the latent heat release, L is found to be independent of the cooling rate. However, the experimental data show that at a fixed temperature, the fraction of heat released at higher cooling rates (5 and 20 °C/min) is lower than that at 1 °C/min for all the solutions studied. We present a model to predict the experimentally measured behavior based on the full set of heat and mass transport equations during the freezing process in a DSC sample pan. Analysis of the parameters relevant to the transport processes reveals that heat transport occurs much more rapidly than mass transport. The model also reveals the important physical parameters controlling the mass transport at the freezing interface i.e., diffusion limited and further elucidates the measured temperature and time dependence of the latent heat release.

Keywords: Phase change; Differential scanning calorimetry; Biological media; Cryoprotective solutions and bound water

1. Introduction

The impetus for study of cryoprotective solutions (solute laden aqueous systems) has been to optimize the preservation of various biological systems. Examples include: blood cell elements for transfusion, pancreatic islets, corneas, tissue and cell cultures for banks and semen for artificial insemination [1,2]. The remarkable success in some systems (blood cell elements, cell cultures, etc.) and the remarkable failure or inadequacy of cryopreservation in other systems (hepatocytes, tissue sections, some mammalian sperm, etc.) have led to much fundamental work on freezing effects within various biological systems as well as work to understand the basic aspects of how certain chemical compounds (cryoprotective media or solute laden aqueous systems) serve to protect cells against undue freezing injury. The following

* Corresponding author. Tel.: +1-612-625-5513; fax: +1-612-624-1398.

E-mail address: bischof@maroon.tc.umn.edu (J.C. Bischof).

[1] Current affiliation: Department of Mechanical Engineering, Louisiana State University, Baton Rouge, LA 70803.

0017-9310/02/$ - see front matter
PII: S0017-9310(01)00290-3

Nomenclature

B	constant cooling rate (K/min)
c	concentration of salt (Osm)
c_l	heat capacitance of the liquid (kJ/kg K)
D	diffusion coefficient (m^2/s)
ε	nondimensional inverse heat transfer coefficient (inverse Fourier number) $(B\overline{R}^2)/(T_{ph0}\alpha_i)$
k	thermal conductivity (W/m K)
K	Nondimensional parameter k_1/k_2
L	latent heat of fusion (J/g)
m	equilibrium constant for a binary solution (obtained from the phase diagram) 1.858 (K/mMol)
Osm	Total moles (disassociated) per liter of solution
M	nondimensional parameter $(mc_0)/T_{ph0}$
v	nondimensional inverse mass transfer diffusivity $(B\overline{R}^2)/(T_{ph0}D_2)$
r	position of freezing front (m)
$\overline{R}$	outer radius of the spherical ice crystals (m)
St	Stefan number $L/(T_{ph0}c_l)$
T	temperature (K)
T_{ph0}	phase change temperature 273.15–mc_0
t	time (min)
μ	viscosity (cP)

Subscripts

i	describes either the frozen or the unfrozen (1 – frozen region) region (2 – unfrozen region)
0	initial value
final	final value

basic/fundamental aspects of freezing solutions have been studied: ice nucleation temperatures [3,4]; curves of homogenous nucleation temperatures as a function of solute concentration [5,6]; and intracellular ice nucleation [7,8]. In addition, the conditions for obtaining a wholly amorphous state by avoiding ice nucleation itself have also been investigated [9]. It is also widely reported in the literature that the amount of 'freezable' water (or water that changes phase during freezing) is less than the total water content, by an amount denoted as the 'bound' or 'unfreezable' water [3,10–12]. The concept of bound water suggests that the latent heat of fusion of the cryoprotective solution is less than that of pure water, as that measured and reported for glycerol solutions [6], phosphate buffer saline solutions [13] and also in NaCl and proline solutions [14]. However, the latent heat of fusion of the cryoprotective solution, a crucial variable in the cryopreservation process, is often approximated to that of pure water (~335 mJ/mg). The nature (magnitude and dynamics) of the latent heat of fusion of several commonly used cryobiological solutions needs to be determined to further our understanding of the freezing process in cryobiology.

The differential scanning calorimeter (DSC) is an instrument that measures heat releases during a phase change process as a function of time and temperature. This instrument is ideally suited to a variety of measurements of the state of water (particularly liquid to solid phase changes) in biological systems and cryoprotective solutions or solute laden aqueous systems [2,6,8,9,13–17]. In the experimental portion of the present study the latent heat of fusion during freezing of various pre-nucleated solute laden aqueous systems is measured using a differential scanning calorimeter (DSC-Pyris 1) at a cooling rate of 5 °C/min. These solutions include: NaCl–H_2O, phosphate buffered saline (PBS), serum-free cell culture media (RPMI), glycerol and anti-freeze proteins (AFPs) in 1x PBS solutions. The latent heat of the 14 different solutions studied is found to be less than that of pure water (~335 mJ/mg) and ranged from 260.0 (±5.0) mJ/mg for 1x (isotonic or 0.3 Osm) NaCl–H_2O solution to 133.0 (±5.0) mJ/mg for 1 Osm glycerol in 1x PBS. Additionally, the dynamics or the temperature (T) and time (t) dependence of the latent heat release is obtained in five commonly used cryobiological media (1x NaCl–H_2O, 10x NaCl–H_2O, 1x PBS, 5x PBS and 10x PBS solutions) by performing DSC experiments at 1 and 20 °C/min. The measured temperature/time dependence in the DSC measured heat release is linked to the rejection of solute (salt) particles during freezing and the consequent reduction of velocity in the liquid–solid interface [18–25].

An examination of the published literature on solidification processes reveals that the temperature (T) and time (t) dependence of the latent heat release can be modeled using one of the two approaches: (1) models of diffusion limited ice crystal growth and (2) heat and mass transfer formulations. The experimental results and models of diffusion limited ice crystal growth (under isothermal as well as nonisothermal conditions) have been published by several investigators [26–34]. In addition, Boutron [9] showed that a model including the interaction of the growing spherical crystals (modeled using Avrami kinetics as detailed in Christian, [35]) can be used to characterize the crystallization kinetics in aqueous solutions. Recently, Smith et al. [36] presented a purely empirical fit to the measured temperature/time dependence of the latent heat release while Devireddy [37] presented a formulation based on Avrami kinetics

to predict the experimentally determined ice crystallization kinetics. [2]

The heat and mass transfer model presented in the numerical portion of the present study (to predict themeasured temperature and time dependence in the latent heat release) is similar to other studies reported in the literature, including Levin [38,39], O'Callaghan and Cravalho [40,41] and Körber [42]. Levin [38,39] presented an analysis of unidirectional (planar) freezing of finite domain aqueous solutions and showed that nonuniform concentration profiles can exist within the liquid region. Levin [39] also found that under certain conditions the solidification process may be limited by mass transfer (solute diffusion away from the interface) conditions rather than heat transfer (removal of sensible and latent heat) conditions. The present study also finds that during freezing of a binary solution in a DSC sample pan the time/temperature dependence of the volume of frozen region is determined by mass transfer considerations (the solute rejection and diffusion at the interface) rather than heat transfer considerations.

2. Materials and methods

2.1. Aqueous solutions – biological media

The experiments were conducted using a DSC-Pyris 1 machine (Perkin–Elmer, Newark, CT). The temperature scale of the instrument was calibrated by the melting point of pure ice (273.15 K or 0 °C) and indium (156.7 °C for 99.9% purity), while the enthalpy scale was based on the heat of fusion of pure ice (335 mJ/mg), as described earlier in Devireddy et al. [43]. The latent heat of fusion during freezing was obtained using the DSC in the following solute laden solutions: (i) 1*x* (isotonic or 0.3 Osm) and 10*x* (3.0 Osm) NaCl–H_2O solutions; (ii) 1*x* (0.3 Osm), 5*x* (1.5 Osm) and 10*x* (3.0 Osm) PBS solutions (Celox, Hopkins, MN); (iii) serum-free RPMI culture media (Celox, Hopkins, MN); (iv) cell culture media: RPMI with 20% fetal bovine serum (FBS) and 1% penicillin–streptomycin (Sigma Chemical, St. Louis, MO); (v) 0.05, 0.1, 0.5 and 1.0 Osm glycerol in isotonic PBS solutions; and (vi) AFP solutions (courtesy of Agouron Pharm, San Diego, CA) with concentrations of 0.1, 1 and 10 mg of AFP per ml of isotonic PBS solution. Thus, the latent heat of fusion was obtained for 14 different aqueous solutions as described below.

2.2. Differential scanning calorimeter experiments

The DSC experiments were conducted by placing approximately 9–10 mg of each solution in a standard aluminum DSC sample pan (Perkin–Elmer Corporation, Norwalk, CT). The sample was cooled at 5 °C/min from 4 °C, until ice nucleated in the solution, typically between −6 and −12 °C (observed as a sharp negative peak on the DSC thermogram). The sample was then re-equilibrated at the phase change temperature (based on the initial osmolality of the solution, i.e. $T_{ph0} = 273.15–1.858\ \mathrm{Osm, K}$) for ∼3–5 min. Isothermal equilibrium at the phase change temperature, T_{ph0} will permit the ice crystals to exist but not grow. The pre-nucleated sample was then cooled from 5 °C/min to −50 °C, to obtain the magnitude and the temperature dependence of the heat release (i.e. the thermogram). In the case of 1*x* NaCl–H_2O, 10*x* NaCl–H_2O, 1*x* PBS, 5*x* PBS and 10*x* PBS solutions, experiments were also conducted at two additional cooling rates of 1 and 20 °C/min. [3] The integrated area under the DSC thermograms (assumed to correspond to the latent heat of fusion) was obtained using the DSC-Pyris 1 (Perkin–Elmer Corporation, Norwalk, CT) software either with a sigmoidal or a linear baseline, as shown in Fig. 1 and as described in the DSC manual. The choice of the baseline influences the integrated area under the thermogram (i.e. the measured value of latent heat). Although more accurate baseline selections are reported in the literature [44], the simpler sigmoidal and linear baselines were used in this study because of their ease of use and their ability to quickly and reproducibly show the important trends in the data (Table 1). The sigmoidal baseline was drawn between the phase change temperature and ∼ −22°C while the linear baseline was drawn between the phase change temperature and ∼ −40°C, as described in the DSC-Pyris 1 manual (Table 1). As shown in Fig. 1, we found that ⩾97% of the latent heat is released between the phase change temperature, T_{ph0} and ∼ −14 and ∼ −18 and ∼ −22 °C when cooled at 1, 5 and 20 °C/min, respectively. Therefore, the temperature and time dependence of the latent heat release was obtained using a sigmoidal baseline drawn between the phase change

[2] Briefly, the model developed by Devireddy [37] assumed, $\Delta(T,t) = \alpha(T)\beta(t)$, where $\alpha(T) = 1 - (A/(T_{ph0} - T + A))$ [where $T < T_{ph0}$] and $\beta(t) = 1 - \exp(-\kappa t^{v})$ [where $t > 0$]. The equilibrium cooling constant, $A(= 0.53)$, Avrami constant, $\kappa(= 3.3)$ and Avrami time exponent, $v(= 1.5)$ were obtained by curve fitting to the experimentally determined data. t is time in minutes and can be represented as $T_{ph0} - T/B$, where B is the cooling rate (K/min) and T_{ph0} is the phase change temperature of the solute laden aqueous solution at $t = 0$.

[3] The higher cooling rate of 20 °C/ min is within the range of cooling rates (<40 °C/ min) to which the DSC can accurately reproduce heat release signatures. We found that for cooling rates greater than 40 °C/min the DSC heat release measurement spreads out and increases in amount [43]. This inaccuracy could be due to the limitation of the rate at which the phase change process proceeds due to ice crystal growth, as well as the nonlinearity of the resistance within the instrument [43].

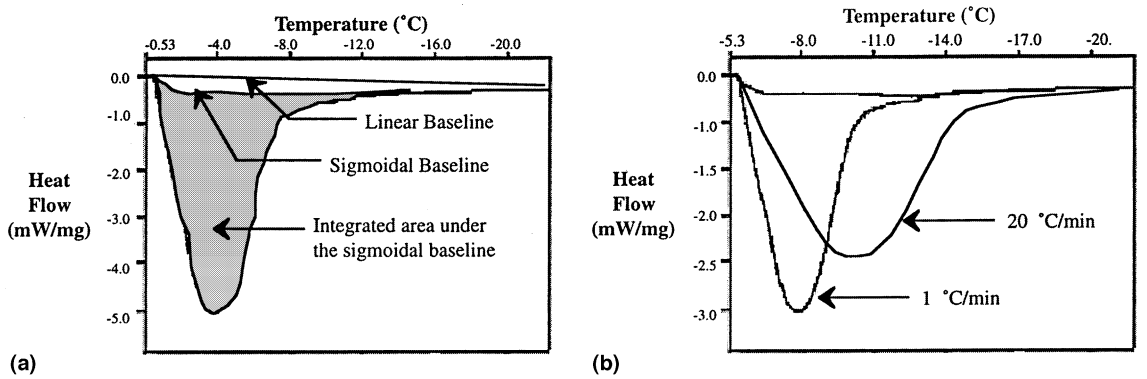

Fig. 1. The DSC measured thermograms are shown for a pre-nucleated solution of 1*x* PBS solution at 5 °C/min (a) and 10*x* PBS solution at 1 and 20 °C/min (b). For illustration, the linear and the sigmoidal baselines are shown in (a). The integrated area under the sigmoidal baseline (shaded region in (a)) represents the DSC measured heat release (latent heat) during freezing. Note that the heat release scale on the *x*-axis is inverted; i.e. negative heat release implies an exothermic heat release. The thermograms show that $\geqslant 97\%$ of the measured heat is released before ~ -18°C at 5 °C/min for 1*x* PBS (a) and before ~ -14°C and ~ -22°C at 1 and 20 °C/min for 10*x* PBS solution (b). Heat flow measured by the DSC is plotted on the *y*-axis while the top *x*-axis represents the temperature.

Table 1
DSC measured heat releases as a function of % dissolved solids in various solute laden aqueous solutions (biological media)

Aqueous system	Magnitude of DSC measured heat release during freezing (J/g)		% Dissolved solids
	Linear baseline (T_{ph} to ~ -40 °C)	Sigmoidal baseline (T_{ph} to ~ -22 °C)	
Pure water[a]	335.0	335.0	0.0
$NaCl$–H_2O:			
0.3 Osm (1*x*)	315.0 ± 5.0	260.0 ± 5.0	0.95 ± 0.05
3.0 Osm (10*x*)	185.0 ± 5.0	152.0 ± 5.0	9.50 ± 0.05
PBS:			
0.3 Osm (1*x*)	304.0 ± 5.0	250.0 ± 5.0	0.95 ± 0.05
1.5 Osm (5*x*)	218.0 ± 5.0	180.0 ± 5.0	5.12 ± 0.07
3.0 Osm (10*x*)	170.0 ± 5.0	140.0 ± 5.0	9.24 ± 0.04
Glycerol in 1x PBS:			
0.05 Osm	290.0 ± 5.0	241.0 ± 5.0	0.90 ± 0.03
0.1 Osm	265.0 ± 5.0	225.0 ± 5.0	1.20 ± 0.05
0.5 Osm	210.0 ± 5.0	175.0 ± 5.0	3.30 ± 0.05
1.0 Osm	160.0 ± 5.0	133.0 ± 5.0	7.90 ± 0.05
RPMI:			
0.3 Osm (Serum-free)	267.0 ± 5.0	220.0 ± 5.0	1.60 ± 0.03
0.3 Osm (Cell culture media)	214.0 ± 5.0	180.0 ± 5.0	1.90 ± 0.06
AFP in 1x PBS:			
3.1×10^{-5} Osm[b]	299 ± 5.0	241 ± 5.0	0.96 ± 0.05[c]
3.1×10^{-4} Osm[b]	294 ± 5.0	236 ± 5.0	1.05 ± 0.05[c]
3.1×10^{-3} Osm[b]	265 ± 5.0	222 ± 5.0	1.95 ± 0.05[c]

[a] DSC was calibrated using these values.
[b] The osmolarity was calculated using a molecular weight of 3242 g/mol for the AFP.
[c] These values were obtained by adding the contribution of dissolved solids originally present in 1*x* PBS and the AFPs in solution.

temperature, T_{ph0} and ~ -14 and ~ -18 and ~ -22 °C for the three cooling rates studied. Six separate DSC experiments were performed with each solution for each cooling rate studied.

2.3. Estimation of dissolved solids

The solute weight fraction in various solutions was obtained by measuring the difference in weight between a hydrated and a fully dehydrated solution. A known quantity of solution (10–15 mg) was placed in an oven at 50–60 °C for 3 days to dehydrate it and precipitate the dissolved solids. The weight of the initially dissolved solids in the solution was measured on a Mettler balance. Although the humidity of the environment (including the oven) in which the solutions were placed was not controlled, the close agreement between the expected and the measured amount of dissolved solids in the $1x$, $5x$ and $10x$ PBS solutions (Table 1), lends credence to the measured % (wt basis) of dissolved solids in the glycerol solutions. As a further test, the amount of dissolved solids in $10x$ PBS and 1 Osm glycerol in $1x$ PBS solutions after heating in the oven was measured in the presence of a desiccant (Drierite or 100% calcium sulfate; Hammond Drierite, Xenia, OH) and was found to be within $\pm 0.1\%$ of the value obtained in the absence of a desiccant. Assuming these samples as a worst case, it is thus suggested that the environmental humidity had a negligible effect ($\pm 0.1\%$) on the measured values of the dissolved solids in the various aqueous solutions. A set of six samples was used for each solution to determine the weight of dissolved solids.

3. A model of freezing of a binary salt solution in a small container

As stated earlier, DSC experiments were conducted at three different cooling rates (1, 5 and 20 °C/min) for five different solutions ($1x$ NaCl–H_2O, $10x$ NaCl–H_2O, $1x$ PBS, $5x$ PBS and $10x$ PBS solutions). The total magnitude of the latent heat release was found to be statistically constant (a variation of less than 2% in the measured value) for a given solution at the three cooling rates studied. However, there was a difference in the temperature and time dependence to the measured value of the latent heat release. We hypothesized that this temperature and time dependence was due to the solute diffusion limitations at the advancing solid front, which we attempted to model as described below.

3.1. The full system: growth of spherical nuclei

To theoretically study the freezing of a binary salt solution in a small container (a DSC sample pan) we consider a heat and mass diffusion model. We assume: (1) A set of identical spherical ice crystals is present initially, and ice grows spherically from these crystals upon further cooling. The choice of spherical ice crystal growth is made because the growth of spherulites during ice crystallization in aqueous solutions (>10 Osm solutions) has been previously observed using an optical-DSC setup [30,45]. We note that cylindrical or planar ice crystal growth geometries may also be considered in the context of our model. While the choice of geometry does not alter our conclusions regarding the roles of heat and mass transport, it does impact the definition of model parameters, ε_i and v_2 defined in Eqs. (13) and (14), respectively. (2) Moreover, we will suppose the size and number of the ice crystals depends on the initial concentration of solutes in the specimen, c_0. This assumption is based on the data obtained in our laboratory (Fig. 2). Fig. 2 also shows that the ice crystals are 'closed' shapes suggesting either a cylindrical or spherical ice crystal growth geometry. (3) There is no interaction among the growing ice crystals, so each ice crystal grows in its own 'pool' of liquid. This assumption allows us to model the behavior of an ensemble of ice crystals by looking at a single ice crystal. This assumption will break down in the late stages of solidification when the normalized frozen fraction nears 1 and there is significant interaction among the ice crystals; however, it is a reasonable way of finding the early time behavior of the latent heat release as a function of the sub-zero temperature.

Based on these assumptions, we establish the following mathematical model. Let $R(t)$ be the radius of the spherical ice crystals (freezing front) at time t. Let $\overline{R}$ be the maximum outer radius of the spherical ice crystal. That is $\overline{R}$ sets a characteristic volume of solution that can be frozen during an experiment. $\overline{R}$ depends on the amount of seed (or initial) ice crystals present at the beginning of freezing, which in turn is dependent on the initial concentration of solutes (Fig. 2). However, $\overline{R}$ is independent of time. Then the governing dimensional equations are:

$$\frac{\partial T}{\partial t}(r,t) = \alpha_i \frac{1}{r^2}\frac{\partial}{\partial r}\left(r^2 \frac{\partial T}{\partial r}\right) \quad \text{for } i = 1,2, \tag{1}$$

$$\frac{\partial c}{\partial t}(r,t) = D_i \frac{1}{r^2}\frac{\partial}{\partial r}\left(r^2 \frac{\partial c}{\partial r}\right) \quad \text{for } i = 1,2, \tag{2}$$

where $i = 1$ denotes the frozen region, $0 \leqslant r \leqslant R(t)$ and $i = 2$ denotes the unfrozen region, $R(t) \leqslant r \leqslant \overline{R}$; α_i, and D_i denote the thermal and compositional diffusivities, respectively. The boundary conditions at the freezing (solute) front boundary $r = R(t)$ are:

$$T(R^+(t),t) = T(R^-(t),t) = T_{ph} = 273.15 - mc(R^+(t),t), \tag{3}$$

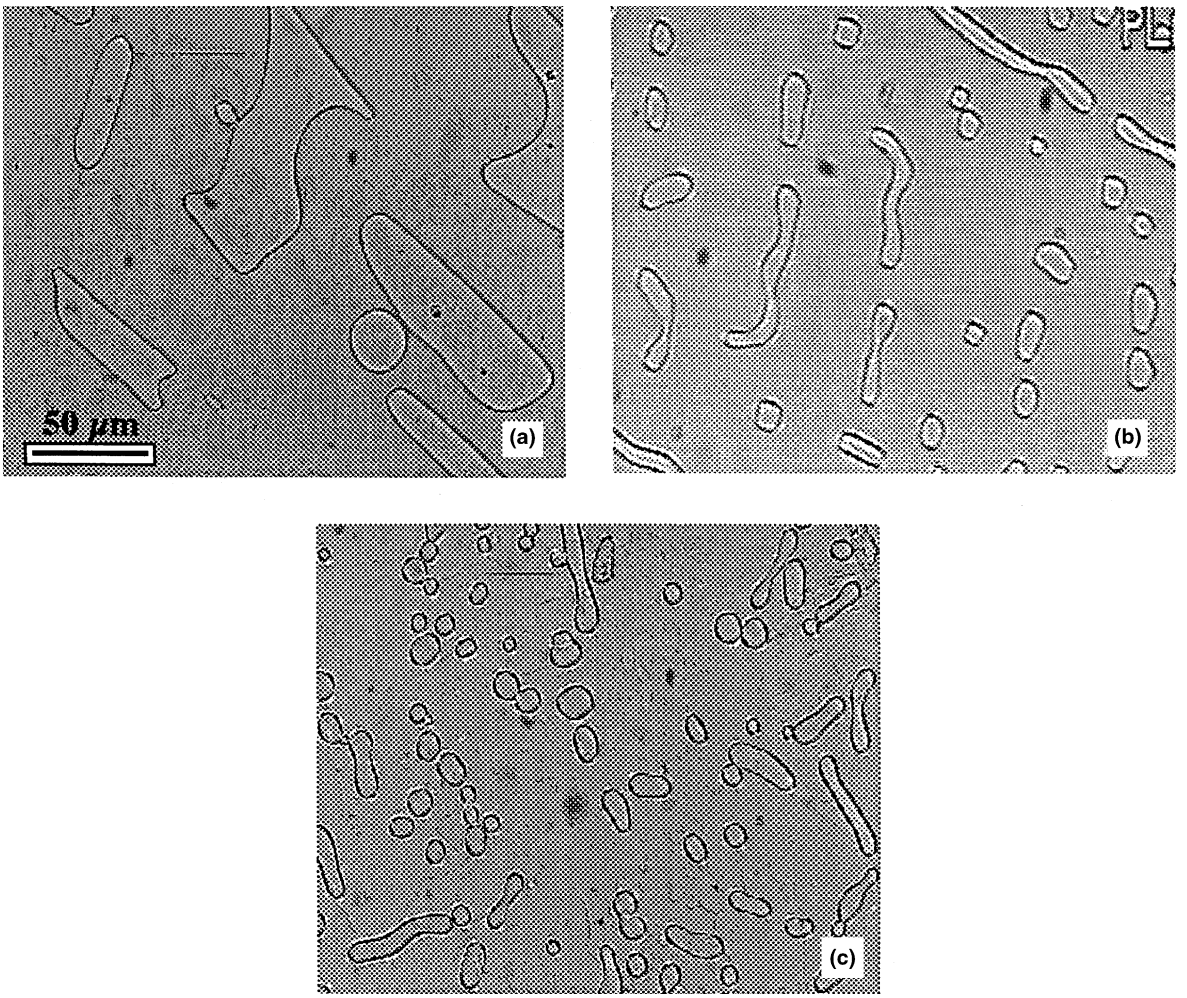

Fig. 2. (a)–(c) show the light micrographs obtained using a cryomicroscope for 1x, 5x and 10x PBS solutions, respectively. A detailed description of the stage and the microscope is provided elsewhere [50]. Clearly, the ice crystals are larger in the 1x PBS solution and are more numerous in the 10x PBS solution.

$$L\frac{\mathrm{d}R}{\mathrm{d}t} = k_1\frac{\partial T}{\partial r}(R^-(t),t) - k_2\frac{\partial T}{\partial r}(R^+(t),t), \tag{4}$$

$$\{c(R^+(t),t) - c(R^-(t),t)\}\frac{\mathrm{d}R}{\mathrm{d}t} = D_2\frac{\partial c}{\partial r}(R^+(t),t) - D_1\frac{\partial c}{\partial r}(R^-(t),t), \tag{5}$$

where $T(R^+(t),t) = \lim_{r\to R^{\pm}(t)} T(r,t)$ and $m(=1.858)$ is the equilibrium constant, k is the thermal conductivity and L is the latent heat of fusion. Eq. (3) specifies the phase change temperature at the freezing interface based on the solute concentration. Eq. (4) states that the difference between the heat flux leaving the solid–liquid interface is the latent heat, L while Eq. (5) describes the rejection and subsequent diffusion of solute at the solid–liquid interface. The initial and the boundary conditions at $r = \overline{R}$ are:

$$T(\overline{R}(t),t) = T_{\mathrm{ph0}} - Bt, \tag{6}$$

where B is the cooling rate and t is the time,

$$\frac{\partial T}{\partial r}(\overline{R},t) = 0 \quad \text{(Neumann)}, \tag{7}$$

$$\frac{\partial c}{\partial r}(\overline{R},t) = 0 \quad \text{(Neumann)}. \tag{8}$$

We also set the concentration at the center of the ice crystal as

$$c(0,t) = 0. \tag{9}$$

Finally, the initial condition at time $t = 0$ in the DSC sample container is

$$c(r,0) = c_0. \tag{10}$$

3.2. Assumptions and nondimensionalization

To simplify the model further, we make the following assumptions: (1) Solute diffusion in the ice is negligible, i.e. $D_1 = 0$. (2) The frozen region has completely rejected the solute, so $c(r,t) = 0$ for $0 \leqslant r \leqslant R(t)$. We note that we have included 'solute trapping' in our models, but unreasonably high amounts of trapping (>80%) need to occur for our model simulations to be significantly affected (data not shown). Such high amounts of solute trapping were thought to be unlikely and therefore, solute trapping is not included in our model.

We then introduce the following dimensionless parameters: $T' = T/T_{\mathrm{ph0}}$, $c' = c/c_0$, $t' = (tB)/T_{\mathrm{ph0}}$ and $r' = r/\overline{R}$. Here c_0 is the initial concentration of solute, and T_{ph0} is the phase change temperature at this concentration, i.e. $T_{\mathrm{ph0}} = 273.15 - mc_0$. We note that both c_0 and T_{ph0} are constants for a given experiment. We also comment that it would be possible to normalize temperature as, $T' = (T - T_2)/(T_{\mathrm{ph0}} - T_2)$, where T_2 is some arbitrarily chosen temperature (for example, we might pick $T_2 = -22$ °C or -40 °C, which are the end temperatures used to analyze the DSC thermograms). However, we found that the choice of nondimensionalization does not affect the results of the model in any way (data not shown).

The nondimensional system is now given by the following field equations (for simplicity we drop the primes on the nondimensional variables)

$$\varepsilon_i \frac{\partial T}{\partial t} = \frac{1}{r^2}\frac{\partial}{\partial r}\left(r^2 \frac{\partial T}{\partial r}\right), \tag{11}$$

$$v_2 \frac{\partial c}{\partial t} = \frac{1}{r^2}\frac{\partial}{\partial r}\left(r^2 \frac{\partial c}{\partial r}\right), \quad R(t) \leqslant r \leqslant 1. \tag{12}$$

The boundary conditions can similarly be nondimensionalized. The nondimensional parameter ε_i is denoted as the inverse heat transfer coefficient (and more traditionally, as the inverse Fourier number, $1/Fo$)

$$\varepsilon_i = \frac{B\overline{R}^2}{T_{\mathrm{ph0}}\alpha_i} \tag{13}$$

while the nondimensional parameter v_2 is denoted as the inverse mass transfer coefficient

$$v_2 = \frac{B\overline{R}^2}{T_{\mathrm{ph0}}D_2}. \tag{14}$$

As $\varepsilon_i(v_2)$ decreases, the effective rate of heat (mass) transport increases. Note also that these nondimensional parameters, hence effective transport rates, depend not only on the dimensional transport coefficients (α_i, D_2), but also on the cooling rate (B), the characteristic system size $(\overline{R})$ and the phase change temperature (T_{ph0}). As mentioned earlier, the dependence of ε_i and v_2 on $\overline{R}$ will change if cylindrical or spherical ice crystal growth geometries are assumed. More specifically, the quadratic dependence of ε_i and v_2 on $\overline{R}$ shown in Eqs. (13) and (14) will change to a linear dependence on $\overline{R}$ for cylindrical crystal geometry and be independent of $\overline{R}$ for planar growth geometries.

We next make a rough estimate of the nondimensional coefficients ε_i and v_2. We take, based on Bird et al. [46], the solute diffusivity in the liquid as $D_2 \approx 10^{-9}$ m^2/s while the thermal diffusivities are $\alpha_{1,2} \approx 10^{-5}$–$10^{-7}$ m^2/s. We take an upper bound for $\overline{R}$ of 0.25 mm, the height of the solution in the DSC pan (in fact we expect $\overline{R}$ to be much smaller as the system contains many small ice crystals). Finally we note that $1\ ^\circ\mathrm{C/min} \leqslant B \leqslant 20\ ^\circ\mathrm{C/min}$ in this study, and T_{ph0} is ~ 273 K. Based on these numbers, we estimate that ε_i ranges from 10^{-4} to 10^{-6} while v_2 ranges from 10^0 to 10^{-2}.

Recalling that ε_i is an inverse heat transfer coefficient (inverse Fourier number) and noting that $\varepsilon_i \ll 1$, we argue that the heat transfer occurs so rapidly that the temperature is constant throughout the system (in contrast to the solute diffusion). Alternatively, if the time dependent term in Eq. (11) is set to zero, the solution to the resulting steady-state equation consistent with the boundary conditions is $T(r,t) = \text{constant in } r$. Noting that the ratio that results from the nondimensionalization of Eq. (4) is finite, i.e., $L/(T_{\mathrm{ph0}} \cdot c_1)$ is finite and $\varepsilon_i \ll 1$, one argues that to within the order of the approximation, Eq. (4) is satisfied for any $\mathrm{d}R(t)/\mathrm{d}t$. Physically, this implies that diffusion of solute away from the interface controls the motion of the interface as the diffusion of heat from the interface is very rapid.

3.3. Reduced system

We now consider the solution of the concentration problem in order to determine the kinetics of solute transport from the growing ice and how it regulates the growth of ice crystals. Solute diffusion is given by

$$v_2 \frac{\partial c}{\partial t} = \frac{1}{r^2}\frac{\partial}{\partial r}\left(r^2 \frac{\partial c}{\partial r}\right), \quad R(t) \leqslant r \leqslant 1. \tag{15}$$

The appropriate boundary conditions are:

$$T(R^{\pm}(t), t) = T_{\mathrm{ph}} = 1 - M(c(R^{+}(t), t) - 1), \tag{16}$$

$$0 = K\frac{\partial T}{\partial r}(R^{-}(t), t) - \frac{\partial T}{\partial r}(R^{+}(t), t), \tag{17}$$

$$v_2 \frac{\partial r}{\partial t} = \frac{-1}{c(R^{+}(t), t)}\frac{\partial c}{\partial r}(R^{+}(t), t), \tag{18}$$

$$T(1,t) = 1 - t, \tag{19}$$

$$\frac{\partial T}{\partial r}(1,t) = 0, \tag{20}$$

$$\frac{\partial c}{\partial r}(1,t) = 0, \tag{21}$$

where $(M = mc_0/T_{ph0})$ and $K = k_1/k_2$. Note that Eqs. (16)–(21) are obtained by nondimensionalization of Eqs. (3)–(8), respectively, with the appropriate assumptions.

The initial conditions are:

$$T(r,0) = c(r,0) = 1. \tag{22}$$

The solution for the temperature field is:

$$T(r,t) = 1 - t. \tag{23}$$

Using this temperature field in Eq. (16), we find that

$$c(R^+(t),t) = 1 + \frac{t}{M}. \tag{24}$$

Also from Eq. (18) the growth of the spherical ice crystals is now given by

$$\frac{dR}{dt} = \frac{1}{v_2}\left[\frac{1}{c(R^+(t),t)}\right]\frac{\partial c(R^+(t),t)}{\partial r} = -\frac{1}{v_2}\left[\frac{1}{1+(t/M)}\right]\frac{\partial c(R^+(t),t)}{\partial r}. \tag{25}$$

The solution of Eq. (25) with the appropriate boundary conditions $((\partial c/\partial r)(\overline{R},t) = 0$, Eq. (24)) was obtained using numerical techniques. Briefly, the numerical code uses a conservative, explicit finite difference scheme to solve the concentration field ahead of the advancing solid/liquid interface. The scheme is second-order accurate in space and first-order accurate in time. A second-order time step stability constraint $(\Delta t \approx \Delta r^2)$ is imposed dynamically by adapting Δt to account for the clustering of grid points in the physical domain as the liquid solidifies.

3.4. Determination of the inverse compositional diffusivity

The variation of v_2 (the only variable in our model solution, Eq. (25)), between the different solutions investigated should be responsible for the experimental temperature/time dependence in the DSC measured heat release (Fig. 4). As shown in Eq. (14), v_2 is dependent on three variables (B, $\overline{R}$ and D_2). We first attempted to model the measured temperature/time dependence in the latent heat release by assuming a temperature dependence for solute diffusion, $D_2(T) = (k/6\pi R)(T/\mu)$ [47]. Using $D_2(298) = 2.83 \times 10^{-11}$ m^2/min and viscosity $(\mu) = 1$ cP we obtain the value of $\frac{k}{6\pi R}$ as 1.58×10^{-15} (kg m/K sec^2). For the viscosity model, we assumed: $\mu = A e^{F/RT}$ where $A = 6.627 \times 10^{-4}$ cP, $F = 1.807 \times 10^4$ kJ/kmol and $R = 8.314$ kJ/kmol K [46]. [4] Thus, a temperature dependence is included in the calculation of the dimensional diffusion coefficient $(D_2(T))$ and consequently in the nondimensional diffusion coefficient (v_2). However, this approach was found to be inadequate to predict the experimental behavior (data not shown). Numerical simulations also showed that the model solution (Eq. (25)) is not significantly affected (<2% variation) when the value of D_2 is either increased or decreased 10-fold (i.e. 10^1 to 10^{-1}), thus, suggesting that the model solution (Eq. (25)) is not particularly sensitive to the value of D_2. Since the other variable, the cooling rate B is set by the experiment, we concluded that the variation in the measured experimental behavior must be due to variations in the characteristic system size, $\overline{R}$.

Table 2
The values of v_2 used in the numerical model

Aqueous system	1 °C/min	5 °C/min	20 °C/min
1x PBS	0.08	0.4	1.6
5x PBS	0.01	0.05	0.2
10x PBS	0.006	0.03	0.12

If $\overline{R}$ is found to be dependent on the solute concentration then the heat and mass diffusion model described above might be used to predict the experimental data. Hence, we investigated the dependence of $\overline{R}$ on the initial concentration of solutes in the solution using a cryomicroscopy stage. Cryomicroscopy images were obtained using a cooling protocol similar to the one used in the DSC experiments, i.e. the sample was supercooled to nucleate ice and then re-equilibrated at the phase change temperature. A detailed description of the stage and the microscope is provided elsewhere [50]. The cryomicroscopy images (Fig. 2) clearly showed that there are larger but fewer ice crystals in the 1x PBS (Fig. 2(a)) than in the 10x PBS solution (Fig. 2(c)), with the number of ice crystals in 5x PBS being intermediate (Fig. 2(b)). The images suggest that with an increase in initial solute concentration, the characteristic length scale decreases, i.e. $\overline{R}_{10x\text{PBS}} < \overline{R}_{5x\text{PBS}} < \overline{R}_{1x\text{PBS}}$; hence, the ratio of surface area to volume also increases.

A simple stereological analysis was performed using NIH™ image analysis software (NIH, Bethesda, MD) to estimate the initial radii of the ice crystals, $R(0)$ at the phase change temperature (T_{ph0}). We found that the initial radius of the ice crystals are $\sim 2.7 \pm 0.1$ and $\sim 3.7 \pm 0.05$ times smaller in the 5x and 10x PBS solution than in the 1x PBS solution, respectively. If one further assumes that $\overline{R}$ scales as the initial radius, $R(0)$, then the value of $\overline{R}$ for 5x and 10x PBS should be lower by a factor of 2.7 and 3.7 times than the value of $\overline{R}$ for 1x PBS solution, respectively. The base value of v_2 was obtained by fitting the numerical (FORTRAN) solution of Eq. (20) to the experimental data for 1x PBS at 1 °C/min using a least-square minimization technique, described in Bevington and Robinson [51]. The resulting fit is shown in Fig. 4(a) and has a goodness of fit pa-

[4] The viscosity (μ) model used in the present study predicts a 10-fold increase in the value of μ between 0 °C and −40 °C which correlates reasonably well with the measured values [47]. Other viscosity models [48,49] also predict a similar increase over the temperature range of interest.

rameter, $R^2 \sim 0.95$. The values of v_2 for $1x$ PBS at higher cooling rates was proportionally increased as defined in Eq. (14). The value of v_2 for $5x$ and $10x$ PBS solutions were obtained by scaling $\overline{R}$ as described above. The values of v_2 for the various cases are shown in Table 2. [5]

4. Results

4.1. Magnitude of latent heat release

The DSC measured heat release magnitudes, L, for the various aqueous systems are shown in Table 1. In general, there is a decrease in heat release as the amount of dissolved solids (solutes) increases. Table 1 shows that isotonic PBS has $\sim 0.9\%$ (by wt) of dissolved solids, which agrees with the expected value based on the isotonic osmolality of 0.3 Osm (typically the % of dissolved solids is also noted on the bottle label). The dissolved solid fraction increases correspondingly at $5x$ and $10x$ PBS to ~ 4.5 and $\sim 9\%$, respectively. The predicted latent heat release based on the total water content for $1x$ PBS is ~ 332 mJ/mg, which is considerably higher than the measured value of ~ 304 mJ/mg (linear baseline) or ~ 250 mJ/mg (sigmoidal baseline). This decrease in latent heat release might either be due to the decrease in latent heat of water (at lower temperatures) or due to the presence of 'bound' water. By accounting for the temperature dependence of the latent heat release of water [4], one finds that the measured value for $1x$ PBS solution should be ~ 315 mJ/mg. This strongly suggests that the measured decrease in the latent heat is due to the presence of 'bound' or 'unfreezable' water attached to dissolved solids in the aqueous systems, in addition to the known temperature dependence of the latent heat release. Other possible causes for this measured decrease in latent heat value are discussed further in Section 5.

Table 1 shows the DSC measured heat releases for various molarities (0.05, 0.1, 0.5 and 1 Osm) of glycerol in $1x$ PBS. Note that an increase in molarity of glycerol (by considering the osmolarity of the systems) leads to a corresponding decrease in the DSC measured latent heat release. Although the addition of AFPs in $1x$ PBS solution did decrease the measured value of latent heat release, the effect of AFP was not as significant as that of glycerol (by considering the moles of solute in solution).

[5] An examination of Eq. (14) shows that the values for v_2 in Table 2 can also be achieved by decreasing viscosity, μ (and consequently increasing diffusivity, D_2) as the concentration of initial solute increases. However, a decrease in viscosity (or an increase in diffusivity, D_2) with increasing solute is contrary to the published literature [47–49]. Therefore, the decrease in v_2 with increasing concentration of solutes must be due to the reduction in $\overline{R}$ (as suggested by cryomicroscopy images shown in Fig. 2).

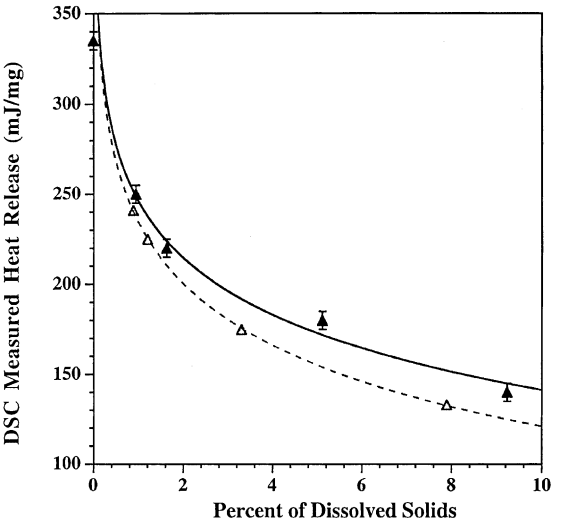

Fig. 3. A comparison of the DSC measured heat releases (sigmoidal baseline; Table 1) between the PBS and glycerol solutions as a function of % dissolved solids (wt basis). The filled triangles (▲) from left to right represent pure distilled water, $1x$ PBS, serum-free RPMI, $5x$ PBS and $10x$ PBS solutions, respectively while the open triangles (△) from left to right represent 0.05, 0.1, 0.5 and 1.0 Osm glycerol in $1x$ PBS solutions, respectively. Note that for $\geqslant 2\%$ dissolved solids in solution, the PBS solutions have ~ 10–15% greater magnitude of latent heat release than the glycerol solutions. The error bars represent standard deviation in the data ($n = 6$ separate DSC experiments).

Therefore, both the 'amount' and 'type' of dissolved solids affect the latent heat of aqueous (solute laden) solutions. This point is illustrated in Fig. 3, which shows a comparison of the DSC measured heat releases (sigmoidal baseline values, Table 1) between the PBS solutions ($1x$, $5x$ and $10x$) and glycerol (0.05, 0.1, 0.5 and 1.0 Osm) in $1x$ PBS solutions. Fig. 3 shows that for solutions with $\geqslant 2\%$ of initially dissolved solids (wt basis), there is ~ 10–15% lower magnitude of heat release during freezing of the glycerol–PBS solutions (△) in comparison to the PBS solutions without glycerol (▲).

4.2. Temperature and time dependence of latent heat release

Figs. 4(a)–(c) show the temperature dependence of latent heat release from $1x$ PBS (0.3 Osm), $5x$ PBS (1.5 Osm) and $10x$ PBS (3.0 Osm) solutions, respectively. In each figure the experimentally determined fraction of heat release at various sub-zero temperatures is shown: 1 °C/min (●); 5 °C/min (■); and 20 °C/min (▲). In Figs. 4(a)–(c), we also present the comparisons between the experimental results and simulations from the

numerical program for the fraction of latent heat released as a function of the sub-zero temperature. The fraction of latent heat released from the numerical model is assumed to be directly proportional to the volume of frozen region and is obtained as the cube of the predicted interface position (i.e. $R(t)^3$). This assumes that the latent heat released is independent of temperature. However, the inclusion of a temperature dependence for the latent heat release [4] did not significantly alter the model simulations (data not shown). Note that both the numerical simulations and the experimental data were normalized such that the fraction of latent heat released is 1 at $T = -14$, -18 and -22 °C for 1, 5 and 20 °C/min, respectively. These temperatures were chosen based on an analysis of the experimental DSC thermograms (as shown in Fig. 1), which showed that $\geqslant 97\%$ of the latent heat is released between the phase change temperature, T_{ph0} and ~ -14 and ~ -18 and ~ -22 °C when cooled at 1, 5 and 20 °C/min, respectively.

To illustrate the effect of the normalization temperature on the experimental and the numerical profiles all

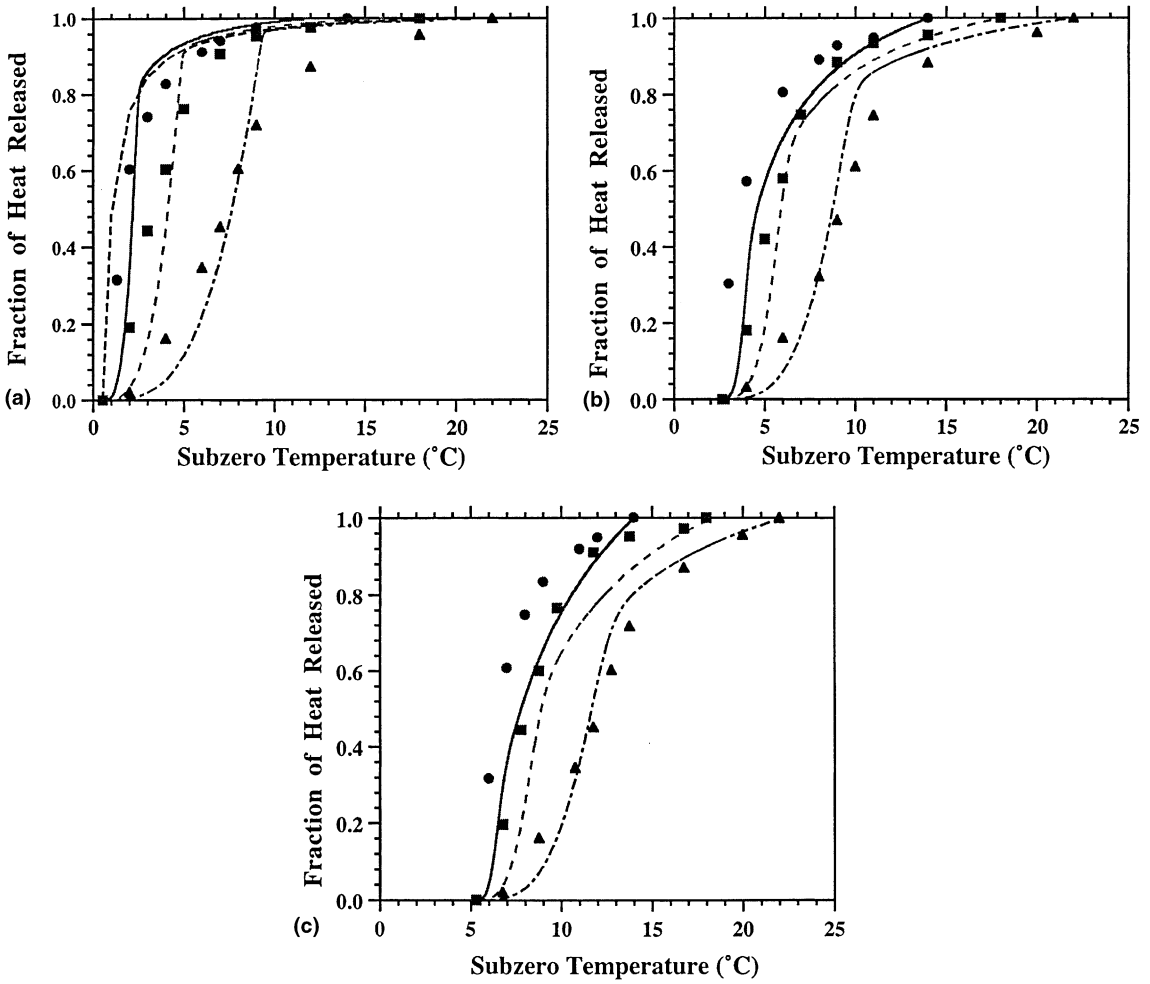

Fig. 4. Temperature and time dependence of the latent heat released during freezing. (a)–(c) show the experimentally determined temperature dependence of latent heat release from 1*x* PBS (0.3 Osm), 5*x* PBS (1.5 Osm) and 10*x* PBS (3.0 Osm) solutions, respectively. In each figure the experimentally (discrete data points) and numerically (continuous lines) determined fraction of heat release at various sub-zero temperatures is shown: 1 °C/min (●, solid curve); 5 °C/min (■, large dashed curve); and 20 °C/min (▲, dotted–dashed curve). Additionally, the innermost dashed curve in (a) corresponds to the fraction of latent heat released that is predicted by the phase diagram [52]. Note that the experimental and the model simulation results have been normalized such that the fraction of heat released is 1 at $T = -14, -18$ and -22 °C for 1, 5 and 20 °C/min, respectively. Error bars are present in the experimental results but are too small to resolve in the graph ($n = 6$ DSC cooling runs at each cooling rate for each solution). Sub-zero temperatures (°C) are shown on the *y*-axis while the fraction of heat released is plotted on the *x*-axis.

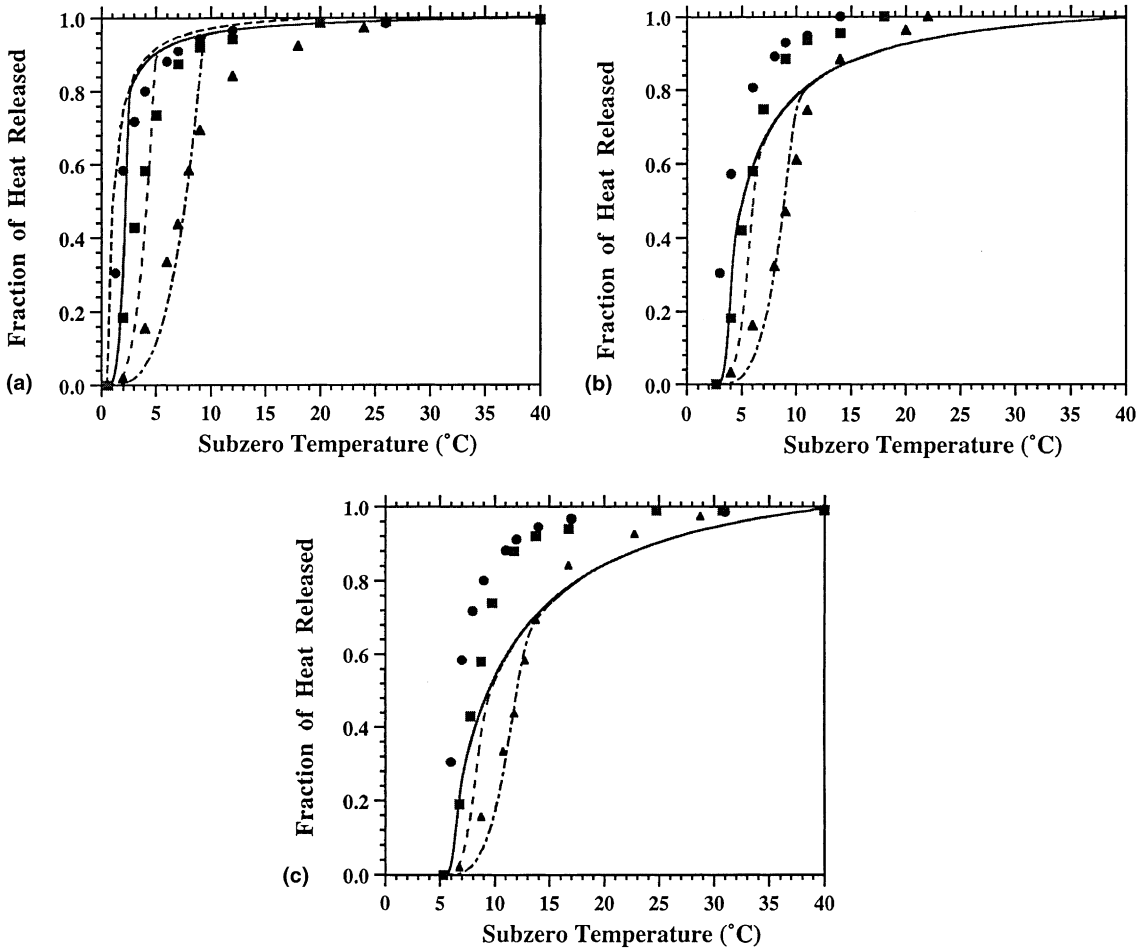

Fig. 5. Temperature and time dependence of the latent heat released during freezing. (a)–(c) show the experimentally determined temperature dependence of latent heat release from 1x PBS (0.3 Osm), 5x PBS (1.5 Osm) and 10x PBS (3.0 Osm) solutions, respectively. In each figure the experimentally (discrete data points) and numerically (continuous lines) determined fraction of heat release at various sub-zero temperatures is shown: 1 °C/ min (●, solid curve); 5 °C/ min (■, large dashed curve); and 20 °C/ min (▲, dotted–dashed curve). Additionally, the dashed curve in (a) corresponds to the fraction of latent heat released that is predicted by the phase diagram [52]. Note that the experimental and the model simulation results have been normalized such that the fraction of heat released is 1 at $T = -40$ °C. Error bars are present in the experimental results but are too small to resolve in the graph ($n = 6$ DSC cooling runs at each cooling rate for each solution). Sub-zero temperatures (°C) are shown on the y-axis while the fraction of heat released is plotted on the x-axis.

the DSC thermograms were normalized to a temperature of −40 °C (these curves are shown in Fig. 5). As in Fig. 4, Figs. 5(a)–(c) show the temperature dependence of latent heat release from 1x PBS (0.3 Osm), 5x PBS (1.5 Osm) and 10x PBS (3.0 Osm) solutions, respectively. In each figure the experimentally determined fraction of heat release at various sub-zero temperatures is shown: 1 °C/ min (●); 5 °C/ min (■); and 20 °C/min (▲). A comparison of Figs. 4 and 5 shows that the normalization temperature changes the shape of both the experimental data and the numerical simulation. The shape of the numerical simulation is more significantly affected for the 5x and 10x PBS solutions than for the 1x PBS solution. More importantly, the model suggests that the latent heat is still being evolved at lower sub-zero temperatures than that noted in the experimental results (as shown in Fig. 5).

One explanation for the above discrepancy is possibly due to our choice of diffusion coefficient (or the viscosity). A lower diffusion coefficient (or higher viscosity) will 'shut off' the evolution of the latent heat and result in a better fit between the experimental data and the model. However, we find that an inordinately large decrease (by a factor of 10^{-10}) in the value of the

diffusion coefficient is needed to occur between the temperature range of 0 and −20 °C for this 'shut-off' effect to occur at a temperature comparable to the experimental data (∼ −20 °C). For the solutions studied, such a large decrease in the diffusion coefficient (or a large increase in viscosity) is unsupported by published literature [47–49]. Therefore, we account for this lowering in the diffusion coefficient (and the 'shut-off') by normalizing the model simulations to experimentally determined temperatures (∼ −14 to −22 °C, based on the cooling rate; as plotted in Fig. 4). This approach has also been used previously by Hayes et al. [52].

By accounting for the presence of the dissolved solids (as shown in Table 1) and the temperature dependence of the latent heat release of water [4], the model simulations shown in Fig. 4 can be used to compute the magnitude of latent heat release for the various solutions studied. [6] An analysis of the 1, 5 and 20 °C/min simulations for the three solutions studied showed that the model predicted magnitude of the latent heat release is $\sim 310.2 \pm 12.5$ mJ/mg (1*x* PBS; Fig. 4(a)), $\sim 290.0 \pm 14.1$ mJ/mg (5*x* PBS; Fig. 4(b)) and $\sim 260.0 \pm 6.3$ mJ/mg (10*x* PBS; Fig. 4(c)). Note that a similar analysis of simulations shown in Fig. 5 was also performed to compute the magnitudes of the predicted latent heat release for the various solutions studied (as shown in Table 3).

A comparison of the predicted and measured latent heat release is shown in Fig. 6. The experimentally measured values in Fig. 6 (●, sigmoidal baseline; ○, linear baseline; shown in Table 1) are significantly lower (∼ 30–50%) than the model predicted values (■; computed using the simulations shown in Fig. 4), with the exception of 1*x* PBS (where the model predicted value compares quite closely with the measured value obtained using the linear baseline). Several possible reasons for this discrepancy are described in Section 5. However, it is important to note that the model predicted latent heat magnitude values also show a trend that is similar to that observed in the experimental results (i.e., an increase in initial solutes causes a concomitant decrease in the predicted/measured latent heat value).

Both the experimental and model results (Figs. 4 and 5) show that the fraction of latent heat release shifts to lower sub-zero temperatures as the cooling rate increases. At a fixed sub-zero temperature, the experimentally determined fraction of heat release at higher cooling rates (5 and 20 °C/min) is lower than that at 1 °C/min, for all the solutions studied. DSC experiments have confirmed that this result was not due to thermal lag in the instrument or machine limitations

[6] Note that the model solution (Eq. (25)) is independent of the magnitude and the temperature dependence of the latent heat release.

Table 3
The computed magnitude of the latent heat release, *L* from the model simulations (Figs. 4 and 5)[a]

Aqueous system	Using simulations shown in Fig. 4 (mJ/mg)	Using simulations shown in Fig. 5 (mJ/mg)
1*x* PBS	310.2 ± 12.5	307.2 ± 10.4
5*x* PBS	290.0 ± 14.1	263.8 ± 10.2
10*x* PBS	260.0 ± 6.3	225.3 ± 6.9

[a] The computed values were obtained using a temperature dependence of latent heat release [4] and also accounted for the expected decrease in the latent heat magnitude due to the presence of dissolved solids (i.e. the mass occupied by the solutes replaces 'freezable' water).

[43]. Rather, the higher cooling rate data can be explained by the scaling of the parameter v_2 with the cooling rate, *B* (shown in Table 2 and Eq. (14)). An increase in the value of v_2 represents an effective decrease in the mass transport at the advancing solid/liquid front,

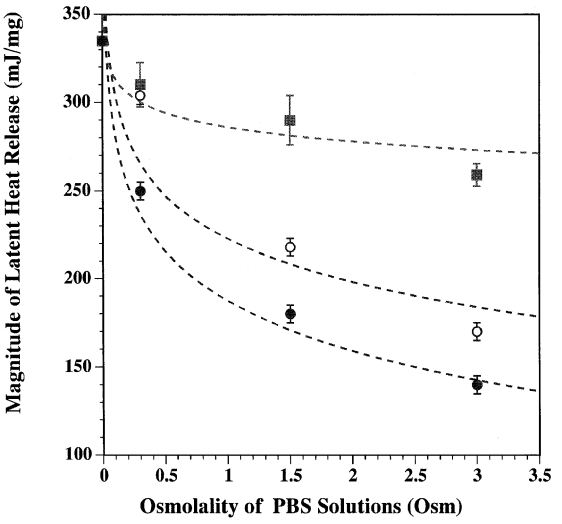

Fig. 6. A comparison of the model predicted and experimentally measured magnitude of latent heat release during freezing of solute laden aqueous solutions (1*x*, 5*x* and 10*x* PBS solutions or 0.3, 1.5 and 3.0 Osm PBS solutions). The experimentally measured values (taken from Table 1) using the DSC are shown as filled (●, sigmoidal baseline) and open (○, linear baseline) circles. Note that the discrepancy between the values obtained using the linear (○) and sigmoidal (●) baselines can be attributed to a 'baseline' error. The model predicted values are shown as filled (■) squares and were computed using the simulations shown in Fig. 4 (the exact values are shown in Table 3). Section 5 provides a brief explanation for the discrepancy between the model predicted and the experimentally measured values of latent heat release. The osmolality of the solutions (taken from Table 1) are shown on the *y*-axis while the magnitude of latent heat release is plotted on the *y*-axis.

because the time available to transport solute decreases. Hence solute 'stacks up' at the front, which shifts the freezing to lower temperatures and slows down the rate of solidification.

In contrast, the effective mass transport increases as B decreases, so at a cooling rate of 1 °C/min the system moves toward a uniform composition profile. In Fig. 4(a) (or Fig. 5(a)), the dashed line at the far left is the heat release profile obtained assuming uniform concentration of solute ahead of the freezing front. This dashed line is based on the phase diagram for the water–NaCl binary (0.3 Osm) solution [52] and is called the 'phase diagram' curve for simplicity. Figs. 4(a) and 5(a) show that the experimental and simulation results for 1 °C/min in 1x PBS solution are very close to the phase diagram curve. However, the experimental results at 1 °C/min for the higher concentration solutions (Figs. 4(b) and (c) or Figs. 5(b) and (c)) are slightly above and to the left of the phase diagram curve for these solutions. (The phase diagram curve is essentially equivalent to the 1 °C/min simulations in these cases.) As the phase diagram curve is based on infinitely fast transport of solute ($v_2 \to 0$), there is no clear way to match the experimental data using the model for the 1 °C/min rates in the 5x and 10x solutions. This suggests that there may be some physics in the system that the model is missing such as a nonlinear relationship between temperature and osmolality in the phase diagram at high solute concentrations. In addition, due to the strong (quadratic) dependence of v_2 on $\overline{R}$ (as defined in Eq. (14)), small variations in $\overline{R}$ cause significant changes in the model simulations and the fit. However, a small variation in $v_2(\sim 10\%)$ does not cause a significant ($<2\%$) variation in the normalized model simulations (data not shown). There is also the possibility of error in the measured data due to the limitations of the sigmoidal baseline [44, as shown in Fig. 6].

Interestingly, an examination of the experimental results in Fig. 4 (Fig. 5) shows that the shape of the experimental curve is insensitive to initial concentration of solutes. That is, the experimental data are statistically equivalent for all the five solutions (NaCl and PBS) studied at a given cooling rate if they are plotted as a function of sub-zero temperature $T - T_{\mathrm{ph0}}$ or time t. Thus, the experimental curves seem to be merely shifts of one another with the shift reflecting the lowering of the phase change temperature due to the increased initial concentration of solutes.

Another important observation is that the temperature and time dependence of 1x NaCl–H_2O and 10x NaCl–H_2O are found to be statistically identical to the data presented for 1x and 10x PBS solutions, respectively (data not shown). However, eutectic heat release (~ 8 to 10% of total) was observed during thawing of the 1x NaCl–H_2O and 10x NaCl–H_2O at ~ -21 °C at all the three thawing rates studied (1, 5, and 20 °C/min). No heat release associated with the eutectic was observed during warming of the other solutions studied (note that each solution was thawed at three different warming rates from −50 to 20 °C).

5. Discussion

5.1. Magnitude of latent heat release

The value of latent heat release obtained in this study for the 14 different types of solute laden aqueous solutions is within the range of reported values in the literature for a variety of biomaterials. Murase and Franks [13] report a value of ~ 275–250 mJ/mg during thawing at 5 °C/min of several different phosphate and sodium buffer solutions using a differential scanning calorimeter (DSC-2) while Rasmussen et al. [14] also report similar values for solutions with NaCl and proline. Recently, Iijima [6] reported latent heat values (thawing at 10 °C/min) ranging from 29.3 to 218 mJ/mg for several concentrations of glycerol in solution ranging from 60% to 10% (% wt/v) using a DSC-7. Similarly, Vinson and Jahn [53] report that an increase in the pore-water salinity causes a decrease in the latent heat of fusion of coarse grained soil infused with saline. However, Defay and Sanfield [54] report that the latent heat value of aqueous solutions is unaffected by the addition of NaCl or $CaCl_2$ in solution based on the calculated values of latent heat (obtained using previously reported values of specific heats).

We believe that the measured reduction in latent heat release for solute laden aqueous solutions in comparison to pure water might occur by several different (but possibly linked) mechanisms: (1) temperature effects on the enthalpy change between the liquid and solid phase during supercooling, which reduces the latent heat of water, L, as previously measured [4]; (2) the mass occupied by the solutes replaces 'freezable' water, which would otherwise change phase and release latent heat of fusion; (3) water may be bound to these solutes or dissolved solids in an 'unfreezable' form and thus will not participate in a bulk heat release, which may be influenced by many factors including: shell of hydration or hydrate formations, heats of dissolution, solute redistribution, etc. [7,10,12,55]; and (4) possible entropic effects due to solute ordering of water prior to the phase change, which decreases both entropy and enthalpy in the liquid phase [56].

An important application of the lower value of the latent heat of fusion of solute laden aqueous systems (vs. in pure water) is to increase the amount of solid phase (ice) formed during freezing of an aqueous (solute laden) system as compared to that in pure water, for a specified cooling load [57]. Further effects of lowering the latent heat value and also incorporating the temperature and

time dependence of the latent heat release during a phase change (cryopreservation or cryosurgical) process are reported elsewhere [36]. We have previously reported that the heat release obtained during freezing of membrane intact cells is greater than that of heat released by the same sample with membrane compromised (or lysed) cells [43,58,59]. This is presumably due to the addition of intracellular components to the extracellular solution during the latter cooling run (i.e. with membrane compromised cells) which in turn reduces L. This decrease in the latent heat release might be an important reason as to why the amount of frozen region (cryolesion) is found to be larger with each successive freeze–thaw cycle during cryosurgery, as reported by several investigators, including Gage [60], Gill et al. [61] and Stewart et al. [62].

5.2. Dynamics of latent heat release

The heat and mass transport model presented in this study is adequate to show that the measured temperature/time dependence on the latent heat release during freezing of a binary solution can be described by mass transfer limitations at the advancing ice front. By correlating the model to the experimental data, we have shown that the heat transfer occurs quickly enough so that the temperature gradients in the system are vanishingly small, and so the motion of the front is dominated by transfer of solute across it. This mass transfer can be described by a single dimensionless parameter, given by v_2 in Eq. (14). The value of v_2 includes the cooling rate and the characteristic system size ($\overline{R}$) as well as the dimensional solute diffusivity (D_2). By fitting the value of v_2 to the experimental data for one case ($1x$ PBS at 1 °C/min), we hoped to isolate the effects of the different contributions. For the $1x$ PBS solution, scaling v_2 by the cooling rate alone gives reasonable agreement with the data at higher cooling rates of 5 and 20 °C/min (Fig. 4(a)).

For the $5x$ PBS (and $5x$ NaCl–H_2O) and $10x$ PBS (and $10x$ NaCl–H_2O) solutions we found that the best way to understand the data is by reducing the system size ($\overline{R}$) with increasing concentration of initial solutes in solution (and the associated cooling rate, B). The reduction in the characteristic system size is probably associated with the ice nucleation phenomena in these solutions. Some support (although not conclusive) for the variation in the system size ($\overline{R}$) with initial concentrations comes from the cryomicroscopy experiments (Fig. 2). The use of cryomicroscopy images to model the behavior of solution in an enclosed container (DSC sample pan) is far from ideal; variations in the sample volume, surface characteristics of the container, temperature history, and so on, may all lead to significant differences in the size and distribution of the ice crystals between the cryomicroscope slide and the DSC sample pan. However, we note that our model simulations fit the experimental data reasonably accurately, if we scale the parameter $\overline{R}$ by the size or radius of ice crystals measured directly from the cryomicroscope images. Thus, for the purpose of the present study, the use of the cryomicroscope images was deemed to be reasonable. Other mechanisms such as the temperature dependence of the solute diffusivity, 'solute trapping' and the temperature dependence of latent heat have been considered, but these effects were not significant enough to explain the experimental results (data not shown). [7]

Possible improvements or modifications to the model include: (1) the inclusion of the interaction between the growing ice crystals [35,48,49,63]. This would give better agreement between the model simulations and the experimental data at lower sub-zero temperatures, but will not significantly affect the conclusions of the present study; (2) the inclusion of nucleation models [64–66] to predict the initial size of the ice crystals or $R(0)$, for an improved and accurate estimation of $\overline{R}$; and finally, (3) the inclusion of irregularly shaped initial ice crystals. In addition, the model also does not account for the formation of partial eutectides which might be occurring due to the high concentration of solutes at the advancing phase front and the effect of lattice orientation and anisotropic effects (resulting in preferred growth of ice crystals) or instabilities at the advancing ice front. Further improvements or modifications to the model (based on the above discussion) will be topics for future studies.

6. Conclusion

The latent heat of fusion during freezing of 14 different pre-nucleated solute laden aqueous systems (commonly used cryobiological media) was obtained using a DSC-Pyris 1 and correlated to the amount of initially dissolved solids or solutes in solution. In general, a decrease in DSC measured heat release (in comparison to that of pure water, 335 mJ/mg) was observed with an increasing fraction of dissolved solids in solution. Both the 'amount' and 'type' of solutes (or solids)

[7] The effect of 'solute trapping' in the frozen region was accounted by modifying the concentration profile at the advancing freeze front (see Eq. (24)). We can account for the effect of solute trapping by modifying the concentration profile at the freeze front as, $c(R^+(t),t) = \frac{t/M}{1+t/M-\xi}$ where ξ is the 'trap' parameter, i.e. the ratio of solute trapped in the frozen region to the initial concentration of solutes. The program was suitably modified and the effect of solute trapping on the numerical simulation was investigated. It was found somewhat paradoxically that ξ needs to be inversely proportional to the cooling rate and also quite significant ($\geqslant 80\%$ or $\xi \geqslant 0.8$) before the simulated latent heat profiles are altered in any significant measure.

in solution were found to decrease the measured value of the latent heat of fusion. Several factors which may contribute to the reduction in the heat release measured in the aqueous systems vs. pure water are: (i) temperature effects during supercooling on the enthalpy change between liquid and solid water, (ii) the mass fraction of solids, (iii) 'bound or unfreezable' water due to interaction with these dissolved solids, and (iv) enthalpy–entropy effects. In addition, the latent heat of fusion during freezing of five different pre-nucleated solute laden aqueous solutions is found to have both a temperature (T) and time (t) dependence. A model to describe the freezing of a binary salt solution in a small container (DSC sample pan) was developed to predict the experimentally determined temperature and time dependence of the latent heat release. The model predicts that the fraction of latent heat released is a decreasing function of cooling rate (as observed in the experimental results). In addition, the model reveals the important physical parameters controlling the freezing process in a solute laden aqueous solution and helps to understand the measured temperature and time dependence of the latent heat release. Clearly, a more fundamental understanding of the microscopic-scale nonhomogeneities in the concentration and thermal fields during freezing of a binary (saline) solution presented in the current study will be of direct relevance to the broader understanding of the full scale freezing (cryopreservation or cryosurgery) problem.

Acknowledgements

This work was supported by grants from the National Science Foundation (NSF – BES # 9703326 and NSF – DMS # 9706831) and a grant from the Materials Research Science and Engineering Center (MRSEC) at the University of Minnesota. We also wish to acknowledge support from the Minnesota Supercomputer Institute. Special thanks to Agouron Pharm, San Diego, CA (in particular, Dr. Ernest Villafranca and Robert Aust) for providing the AFPs.

References

[1] J.J. McGrath, Preservation of biological material by freezing and thawing, in: A. Shitzer, R.C. Eberhart (Eds.), Heat Transfer in Medicine and Biology, Plenum Press, New York, 1985, pp. 185–238.

[2] J.C. Bischof, Quantitative measurement and prediction of biophysical response during freezing in tissues, Annu. Rev. Biomed. Eng. 2 (2000) 257–288.

[3] F. Franks, The properties of aqueous solutions at subzero temperatures, in: F. Franks (Ed.), Water, A Comprehensive Treatise, vol. 7, Plenum Press, New York, 1982, pp. 215–338.

[4] P.V. Hobbs, in: Ice Physics, Clarendon, Oxford, 1974, pp. 361–362.

[5] A.P. MacKenzie, Non-equilibrium freezing behaviour of aqueous systems, Philos. Trans. R. Soc. London 278 (1977) 167–189.

[6] T. Iijima, Thermal analysis of cryoprotective solutions for red blood cells, Cryobiology 36 (1988) 165–173.

[7] F. Franks, Solute-water interactions: do polyhydroxy compounds alter the properties of water?, Cryobiology 20 (1983) 335–345.

[8] C.H. Körber, S. Englich, G. Rau, Intracellular ice formation: cryomicroscopical observation and calorimetric measurement, J. Microsc. 161 (1991) 313–325.

[9] P. Boutron, Comparison with the theory of the kinetics and extent of ice crystallization and of the glass-forming tendency in aqueous cryoprotective solutions, Cryobiology 23 (1986) 88–102.

[10] T. Moran, The freezing of gelatine gel, Proceedings of the Royal Society (London) 112A (1926) 30–46.

[11] O.R. Fennema, W.D. Powrie, E.H. Marth, in: Low-temperature Preservation of Foods and Living Matter, Marcel Dekker, New York, 1973, pp. 63–66.

[12] R. Cooke, I.D. Kuntz, The properties of water in biological systems, Annu. Rev. Biophys. Bioeng. 3 (1974) 95–126.

[13] N. Murase, F. Franks, Salt precipitation during the freeze-concentration of phosphate buffer solutions, Biophys. Chem. 34 (1989) 293–300.

[14] P.H. Rasmussen, B. Jorgensen, J. Nielsen, Aqueous solutions of proline and NaCl studied by differential scanning calorimetry at subzero temperatures, Thermochim. Acta 303 (1997) 23–30.

[15] R.J. Williams, H.T. Meryman, A calorimetric method for measuring ice in frozen solutions, Cryobiology 1 (1965) 317–323.

[16] Z. Chang, T.N. Hansen, J.G. Baust, The effect of antifreeze proteins on the devitrification of a cryoprotective system, Cryo-Letters 12 (1991) 215–226.

[17] T.W. Schenz, B. Israel, M.A. Rosolen, Thermal analysis of water-containing systems, in: H. Levine, L. Slade (Eds.), Water Relationships in Food, Plenum Press, New York, 1991, pp. 199–214.

[18] B. Rubinsky, E.G. Cravalho, An analytical method to evaluate cooling rates during cryopreservation protocols, Cryobiology 21 (1984) 303–320.

[19] K. Wollhöver, C.H. Körber, M.W. Scheiwe, U. Hartmann, Unidirectional freezing of binary aqueous solutions: an analysis of transient diffusion of heat and mass, Int. J. Heat Mass Transfer 28 (4) (1985) 761–769.

[20] V.G. Smith, W.A. Tiller, J.W. Rutter, A mathematical analysis of solute redistribution during freezing, Can. J. Phys. 33 (1955) 723–745.

[21] J.P. Terwilliger, S.F. Dizio, Salt rejection phenomena in the freezing of saline solutions, Chem. Eng. Sci. 25 (1970) 1331–1349.

[22] B.W. Grange, R. Viskanta, W.H. Stevenson, Diffusion of heat and solute during freezing of salt solutions, Int. J. Heat Mass Transfer 19 (1976) 373–384.

[23] C.H. Körber, M.W. Scheiwe, K. Wollhöver, Solute polarization during planar freezing of aqueous salt solutions, Int. J. Heat Mass Transfer 26 (8) (1983) 1241–1253.

[24] S. Kourosh, K.R. Diller, M.E. Crawford, Microscopic study of coupled heat and mass transport during unidirectional solidification of binary solutions – I. Thermal analysis, Int. J. Heat Mass Transfer 33 (1) (1990) 29–38.
[25] S. Kourosh, K.R. Diller, M.E. Crawford, Microscopic study of coupled heat and mass transport during unidirectional solidification of binary solutions – II. Mass transfer analysis, Int. J. Heat Mass Transfer 33 (1) (1990) 39–53.
[26] M. Avrami, Kinetics of phase change. I. General theory, J. Chem. Phys. 7 (1939) 1103–1112.
[27] M. Avrami, Kinetics of phase change. II Transformation-time relations for random distribution of nuclei, J. Chem. Phys. 8 (1940) 212–224.
[28] M. Avrami, Granulation, phase change, and microstructure. Kinetics of phase change III, J. Chem. Phys. 9 (1941) 177–184.
[29] J.W. Cahn, Transformation kinetics during continuous cooling, Acta Metall. 4 (1956) 572–575.
[30] J.M. Hey, D.R. MacFarlane, Crystallization of ice in aqueous solutions of glycerol and dimethylsulfoxide 2: Ice crystal growth kinetics, Cryobiology 37 (1988) 119–130.
[31] P.M. Mehl, Crystallization and vitrification in aqueous glass-forming solutions, in: P.L. Steponkus (Ed.), Advances in Low-Temperature Biology, 3, JAI Press LTD, London, 1996, pp. 185–255.
[32] M. Kresin, C.H. Körber, Influence of additives on crystallization kinetics: comparison between theory and measurements in aqueous solutions, J. Chem. Phys. 95 (1991) 5249–5255.
[33] N. Kubota, J.W. Mullin, A kinetic model for crystal growth from aqueous solution in the presence of impurity, J. Cryst. Growth 152 (1995) 203–208.
[34] Y. Long, R.A. Shanks, Z.H. Stachurski, Kinetics of polymer crystallization, Progr. Polym. Sci. 20 (1995) 651–701.
[35] J.W. Christian, in: The Theory of Transformations in Metals and Alloys, Pergamon Press, New York, 1981, pp. 540–545.
[36] D.J. Smith, R.V. Devireddy, J.C. Bischof, Prediction of thermal history and interface propagation during freezing in biological systems – latent heat and temperature dependent property effects, in: The proceedings of the 5th ASME-JSME Thermal Engineering Joint Conference, San Diego, 1999. CD-ROM Publication http://www.me.umn.edu/divisions/tht/bhmt/publications/pdf/ASMEJSME-freezing.pdf.
[37] R.V. Devireddy, Measurement of freezing processes in biological systems, Ph.D. Thesis, Department of Mechanical Engineering, University of Minnesota, Minneapolis, MN, 1999.
[38] R.L. Levin, Generalized analytical solution for the freezing of a super-cooled aqueous solution in a finite domain, Int. J. Heat Mass Transfer 23 (1980) 951–959.
[39] R.L. Levin, The freezing of finite domain aqueous solutions: solute redistribution, Int. J. Heat Mass Transfer 24 (9) (1981) 1443–1455.
[40] M.G. O'Callaghan, E.G. Cravalho, An analysis of the heat and solute transport during solidification of an aqueous binary solution – I. Basal plane region, Int. J. Heat Mass Transfer 25 (1982) 553–562.
[41] M.G. O'Callaghan, E.G. Cravalho, An analysis of the heat and solute transport during solidification of an aqueous binary solution – II. Dendrite tip region, Int. J. Heat Mass Transfer 25 (1982) 563–573.
[42] C.H. Körber, Phenomena at the advancing ice–liquid interface: solutes, particles and biological cells, Q. Rev. Biophys. 21 (2) (1988) 229–298.
[43] R.V. Devireddy, D. Raha, J.C. Bischof, Measurement of water transport during freezing in cell suspensions using a differential scanning calorimeter, Cryobiology 36 (2) (1988) 124–155.
[44] C.M. Guttman, J.H. Flynn, On the drawing of the baseline for differential scanning calorimetric calculation of heats of transition, Anal. Chem. 45 (1973) 408–411.
[45] J.M. Hey, P.M. Mehl, D.R. MacFarlane, Combined differential scanning calorimeter–optical video microscope for crystallization studies, J. Thermal Anal. 49 (2) (1997) 991–998.
[46] R.B. Bird, W.E. Stewart, E.N. Lightfoot, in: Transport Phenomena, Wiley, New York, 1994, pp. 26–29.
[47] T.K. Eto, B.J. Costello, S.W. Wenzel, R.M. White, B. Rubinsky, Viscosity sensing with lamb-wave microsensor: dimethylsulfoxide solution viscosity as a function of temperature, ASME J. Biomech. Eng. 115 (1993) 329–331.
[48] J.O.M. Karlsson, E.G. Cravalho, I.H.M. Borel Rinkes, R.G. Tompkins, M.L. Yarmush, M. Toner, Nucleation and growth of ice crystals inside cultured hepatocytes during freezing in the presence of dimethylsulfoxide, Biophys. J. 65 (1993) 2524–2536.
[49] J.O.M. Karlsson, E.G. Cravalho, M. Toner, A model of diffusion-limited ice growth inside biological cells during freezing, J. Appl. Phys. 75 (1994) 4442–4445.
[50] M.S. Berrada, J.C. Bischof, A determination of biophysical parameters related to freezing of an ELT-3 cell line, Adv. Heat Mass Transfer Biotechnol. 368 (2000) 41–48.
[51] P.R. Bevington, D.K. Robinson, Data Reduction and Error Analysis for the Physical Sciences, second ed., McGraw-Hill, New York, 1992.
[52] L.J. Hayes, K.R. Diller, H.J. Chang, A robust numerical method for latent heat release during phase change, ASME Heat Transfer Division 62 (1986) 63–69.
[53] T.S. Vinson, S.L. Jahn, Latent heat of frozen saline coarse-grained soil, J. Geotechnical Eng. 111 (1985) 607–623.
[54] R. Defay, A. Sanfield, Chaleur de fusion de la glace en présence d'une solution aquese de sel, Bull. Soc. Chem. Belgium 68 (1959) 295–302.
[55] G. Taborsky, Solute redistribution in some multicomponent aqueous systems on freezing, J. Biol. Chem. 245 (5) (1970) 1063–1068.
[56] R. Lumry, S. Rajender, Enthalpy–entropy compensation phenomena in water solution of proteins and small molecules: a ubiquitous property of water, Polymers 9 (1970) 1125–1227.
[57] H.S. Carslaw, J.C. Jaeger, Conduction of Heat in Solids, second ed., Clarendon Press, Oxford, 1959.
[58] R.V. Devireddy, J.C. Bischof, Measurement of water transport during freezing in mammalian liver tissue – Part II: The use of differential scanning calorimetry, ASME J. Biomech. Eng. 120 (5) (1988) 559–569.

[59] R.V. Devireddy, D.J. Smith, J.C. Bischof, Mass transfer during freezing of rat prostate tumor tissue, AIChE J. 45 (3) (1999) 639–654.
[60] A.A. Gage, Experimental cryogenic injury of the palate: observations pertinent to the cryosurgical destruction of tumors, Cryobiology 15 (1978) 415–425.
[61] W. Gill, J. Fraser, D.C. Carter, Repeated freeze-thaw cycles in cryosurgery, Nature 219 (1968) 410–413.
[62] G.J. Stewart, A. Preketes, M. Horton, W.B. Ross, D.L. Morris, Hepatic cryotheraphy: double-freeze cycles achieve greater hepatocellular injury in man, Cryobiology 32 (1995) 215–219.
[63] M. Rapaz, Modelling of microstructure formation in solidification processes, Int. Mater. Rev. 34 (1989) 93–123.
[64] D. Turnbull, J.C. Fisher, Rate of nucleation in condensed systems, J. Chem. Phys. 17 (1949) 71–72.
[65] M. Toner, E.G. Cravalho, M. Karel, Thermodynamics and kinetics of intracellular ice formation during freezing of biological cells, J. Appl. Phys. 67 (1990) 1582–1593, Erratum: Journal of Applied Physics 10 (1991) 463–465.
[66] B. Rubinsky, Solidification process in saline solutions, J. Cryst. Growth 63 (1983) 513–522.